

CHARACTERIZING THE DEPTHS AND CENTRAL PEAKS OF
LUNAR COMPLEX CRATERS WITH LOLA TOPOGRAPHY

By
JESSICA KALYNN

A THESIS SUBMITTED IN PARTIAL FULFILLMENT OF
THE REQUIREMENTS FOR THE DEGREE OF
BACHELOR OF SCIENCE (HONOURS)
in
THE FACULTY OF SCIENCE
(GEOPHYSICS)

This thesis conforms to the required standard

.....
Supervisor

THE UNIVERSITY OF BRITISH COLUMBIA
Vancouver

MARCH 2012

ABSTRACT

Using recently-released Lunar Orbiter Laser Altimeter (LOLA) topography data, we revisit the depth-diameter and central peak height-diameter relationships for fresh complex lunar craters that previously could only be determined using images. We assembled a dataset of young craters with diameters $\geq 15\text{km}$ and ensured they were unmodified and fresh using Lunar Reconnaissance Orbiter's Wide-Angle Camera images. LOLA's gridded topography data records allowed us to determine the rim-to-floor crater depths, as well as central peak heights above the crater floor, which we analyzed as a function of crater diameter using power law relationships. We find that the depths are deeper and central peak heights are larger than previously reported. Further they are dependent on target terrain - craters on highland terrain are on average deeper and have higher central peaks than craters on mare terrain. There is a significant amount of variability within the central peak heights for a given diameter, which should be investigated in future studies. Viable numerical models for complex crater formation should match our depth-diameter relationships and endeavor to predict the central peak height variability.

TABLE OF CONTENTS

TITLE PAGE	i
ABSTRACT	ii
TABLE OF CONTENTS	iii
LIST OF FIGURES	iv
LIST OF TABLES	v
ACKNOWLEDGEMENTS	vi
INTRODUCTION	1
METHODS	4
2.1 Dataset of Fresh Complex Craters.....	4
2.2 Topography Analyses	6
RESULTS	10
3.1 Depth - Diameter	11
3.2 Central Uplifts	12
3.3 GDR and RDR Variability.....	16
DISCUSSION	16
4.1 Depth – Diameter.....	16
4.2 Central Peak Anomalies	18
FUTURE QUESTIONS	19
REFERENCES	21

LIST OF FIGURES

FIGURE 1	Pike (1981) depth-diameter relationships	2
FIGURE 2	Examples of fresh and modified craters.....	5
FIGURE 3	Geographical distribution of our craters	6
FIGURE 4	Topography of Aristillus crater.....	7
FIGURE 5	Elevation histogram of Aristillus crater	8
FIGURE 6	Topography of Herschel crater.....	9
FIGURE 7	Histograms of craters with and without central peaks	10
FIGURE 8	Depth vs. diameter	11
FIGURE 9	Central peak height vs. diameter plot.....	13
FIGURE 10	Example of typical central peak.....	14
FIGURE 11	Example of low central peak.....	15
FIGURE 12	Example of high central peak.....	15
FIGURE 13	Comparison of GDR/RDR profiles.....	16
FIGURE 14	Central peak height vs. depth plot.....	18
FIGURE 15	Topography and histogram of Rutherford crater	20

LIST OF TABLES

TABLE 1	Constants for depth versus diameter fits.....	12
TABLE 2	Constants for central peak-height versus diameter fits.....	13
TABLE 3	Craters from Pike (1981) still known to be fresh.....	17

ACKNOWLEDGEMENTS

First and foremost I would like to thank Dr. Catherine Johnson for all of the time, support, advice, and opportunities that she has given me. She has been the greatest asset to my degree and I couldn't be more grateful to have her as my advisor.

I would also like to thank Dr. Gordon Osinski at The University of Western Ontario, for his guidance in planetary geology, and Dr. Olivier Barnouin at John Hopkins University for his wealth of knowledge on the cratering process. I am grateful to Richard Pike for providing us with additional background data and materials used in his publications, to Richard Grieve for his useful discussions, and to Dr. Mark Jellinek for teaching me what it means to write.

Lastly, thank you to my family and friends for their patience and encouragement throughout my degree and to my mom and Chris for their unconditional love and support.

1. INTRODUCTION

The formation of impact craters on planetary¹ surfaces is a ubiquitous process on solar system bodies. The impact of an incoming bolide into a solid surface, fragments or even completely destroys the bolide. The target is heated and shocked, and the impact excavates and redistributes pre-existing surface material. The resulting geological structure – the “fresh” impact crater – records the net effects of the impactor (e.g., its mass, size, speed and impact angle) and the properties of the impacted surface/lithosphere (e.g., density and strength). Subsequent tectonic, volcanic, weathering or erosional processes can further modify the impact crater topography and morphology. To first order, impact crater characteristics vary with crater size. Small craters are simple, bowl-shaped structures; intermediate-sized craters have flat floors, terraced walls, and central uplifts and are known as complex craters; large craters can have multiple rings, and are known as basins. Crater “size” is typically measured in terms of the rim-to-rim diameter, where the rim is identified in images and/or topography data. The diameters at which the simple-to-complex, or complex-to-basin, transitions occur have been shown to scale inversely with gravity (Melosh, 1989).

The morphometry of craters is thus important to understanding the cratering process and provides constraints which viable analytical or numerical models for crater formation must match (Melosh, 1989). Much of our understanding of impact craters has been built on observations of lunar craters. On the Moon, the simple-to-complex and complex-to-basin transitions are observed to occur at crater diameters of approximately 30 km and 200 km respectively (Melosh, 1989). Early investigations by Baldwin (1963, 1965) of lunar crater morphometry used shadow lengths in Earth-based imagery to relate “rim-to-rim diameter” to “rim-to-floor” depth. Later, using stereophotogrammetry derived from Apollo metric photos, and shadow lengths from Lunar Orbiter IV photos, Pike established depth (d) – diameter (D) relations for simple and complex craters (Pike, 1974, 1980, 1981). The cumulative results of these studies are shown in Figure 1 and comprise three main points. First, depth increases with diameter, and the d - D curve is well matched by a power law relationship of the form $d = AD^B$, where A and B are constants determined by a linear least squares fit of $\log(d)$ versus $\log(D)$. Second, a change in the d - D relationship is seen at crater diameters around 15 km, roughly coincident with the morphological transition from simple to complex craters. Third,

¹ In this thesis we use the term “planetary” in a generic sense to include planets, moons and asteroids.

craters on the lunar highlands (heavily cratered, ancient surfaces composed dominantly of anorthosite) are typically deeper than those on the lunar mare (younger, basaltic surfaces) at a given diameter.

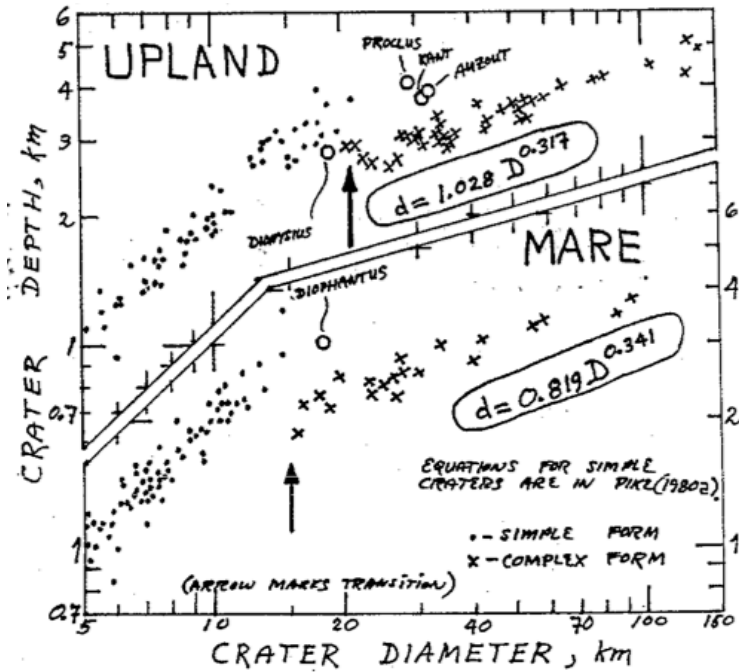


Figure 1 The depth and diameter relationships reported by Pike (1981). Dots indicate "simple" craters (*i.e.*, bowl-shaped craters) and crosses indicate complex craters. The top section of the figure shows craters on upland terrain (the lunar highlands) and the lower section of the figure shows craters on mare terrain. Power law fits for complex craters on the highlands and mare are given. Figure taken directly from Pike (1981).

The first two of these results, together with the corresponding power law fits have guided models for crater formation, and studies of craters on other terrestrial planets for over thirty years. The difference between mare/highlands craters has received less attention, in part because it is poorly understood. A qualitative explanation often quoted in the literature is that the difference reflects differences in strength of the target material (the more heavily fractured highland material being assumed to be weaker than the more intact mare material), but this has not been explored quantitatively.

Other aspects of complex craters have also been investigated such the morphology of the central peak, its height (h_{cp}), diameter area and volume, and how these scale with crater diameter (Wood, 1973; Wood and Head, 1976; Pike, 1977; Wood and Andersson, 1978; Hale and Head, 1979; Hale and Grieve, 1982). Central peak height has also been found to increase with crater diameter up

to a diameter of about 80 km (Hale and Head, 1979), but no significant differences for craters on the mare versus the highlands have been reported.

With the exception of one previous study of lunar basins and large complex craters [8], all previous analyses have been image-based due to the lack of absolute altimetric data of sufficient resolution to characterize crater topography. Lunar Orbiter Laser Altimeter (LOLA) data allow, for the first time, investigations of the absolute topography of lunar complex craters. The most recently-released LOLA gridded data set has a spatial resolution of 1028 pixels per degree or ~ 30 m, close to the maximum along-track resolution of the actual orbit tracks, and has a vertical accuracy of 0.1 m, permitting the study of craters with diameters 10s km and smaller. In particular, the higher vertical precision and accuracy, and higher spatial resolution compared with the previously-available Clementine topography data, (~ 100 m vertical accuracy, maximum along-track spatial resolution of 20 km and a cross-track spatial resolution at the equator of ~ 60 km), are critical to the correct assessment of crater floor and rim elevations, and are required to resolve the topography of central peaks. Image data collected by the Lunar Reconnaissance Orbiter Camera (LROC), have a spatial resolution of up to 0.5 m per pixel for the Narrow Angle Camera and 100 m per pixel for the Wide Angle Camera and allow improved assessment over earlier studies of whether an individual crater is fresh or has been subsequently modified. In addition, LROC data provide global coverage of the moon, whereas previous studies were biased geographically toward the regions covered by the Lunar Orbiter and Apollo images.

In this study we revisit the d - D and h_{cp} - D relationships for lunar complex craters using, for the first time, absolute topography data. Our goal is to characterize unmodified craters, so that the results of use for crater formation models, and so we first establish a data set of complex craters that comprises only young, fresh craters (Section 2.1). We describe how we estimate the crater depth and central peak height from the LOLA topography data (Section 2.2) and we establish new d - D and h_{cp} - D relationships for mare and highland craters (Section 3). We discuss how these results compare with previous studies (Section 4). We conclude with suggested directions for future studies (Section 5).

2. METHODS

2.1 Dataset of Fresh Complex Craters

Our objective is to establish a data set of fresh complex craters that is sufficiently large to statistically characterize changes in crater topography with diameter. Recent studies of the global lunar crater distribution have yielded a new database of latitude, longitude and diameters for 5185 craters with diameters greater than 20 km (Head et al. 2010; Kadish et al., 2011). However, we use as our starting point an earlier database of 8680 craters (Losiak et al., 2009) for two reasons. First, it includes, where available, ancillary information such as crater age. Second, we chose a minimum crater diameter less than 20 km in establishing our initial dataset to ensure that we capture any small diameter complex craters. We selected craters with reported ages that are Eratosthenian (3.2-1.1 Ga) or Copernican (1.1 Ga to present), where the ages are taken from Wilhelms (1987). We excluded craters with diameters less than 15 km, to remove simple craters and some craters that have morphologies transitional between those of simple and complex craters. These selection criteria resulted in a dataset of 140 craters with diameters in the range 15 – 167 km; craters with diameters larger than 167 km are all pre-Eratosthenian.

Wide Angle Camera (WAC) images from the Lunar Reconnaissance Orbiter Camera (LROC) were used to check that our selected craters are “fresh,” as defined below. The WAC monochromatic images of each crater were obtained through the “LROC Image Search” website. These images were then calibrated, inverted and corrected for distortion using freely available software (Mosher, 2010). A crater is considered fresh if the following criteria are met: (1) melt pools are observed in the crater floor, (2) the rim is well-defined, (3) fault scarps are present, and/or (4) striations in the ejecta blanket are evident. Examples of fresh craters are shown in Figures 2a – 2c. A crater is considered to not be fresh if there is evidence for any of the following: (1) subsequent impacting or microbombardment either in its interior (e.g., Figure 2e), or rim, (2) influence by the ejecta of a nearby later crater, (3) modification due to magmatic or tectonic activity (e.g. Figure 2d) and/or (4) an irregular shape (e.g., Figure 2f). Inspection of individual craters indicates that 13 craters are not fresh and we remove these from our database. For 9 additional craters, the WAC images contain significant shadowing that

prevented us from clearly seeing the crater floor. As we were unable to verify that these craters meet our freshness criteria above, we do not include them in our dataset. We supplemented the small number of larger diameter craters by including fresh Upper Imbrium age craters with diameters larger than 80km. Seven of these meet our criteria for fresh craters and add to our dataset. The final list of 118 fresh craters is provided in Supplementary Table 1, and spans the diameter range 15 – 190 km. Figure 3 illustrates the global distribution of these our 118 fresh craters, and shows that our set is a good representation of the lunar surface. Our data set is given in the table in Appendix 1.

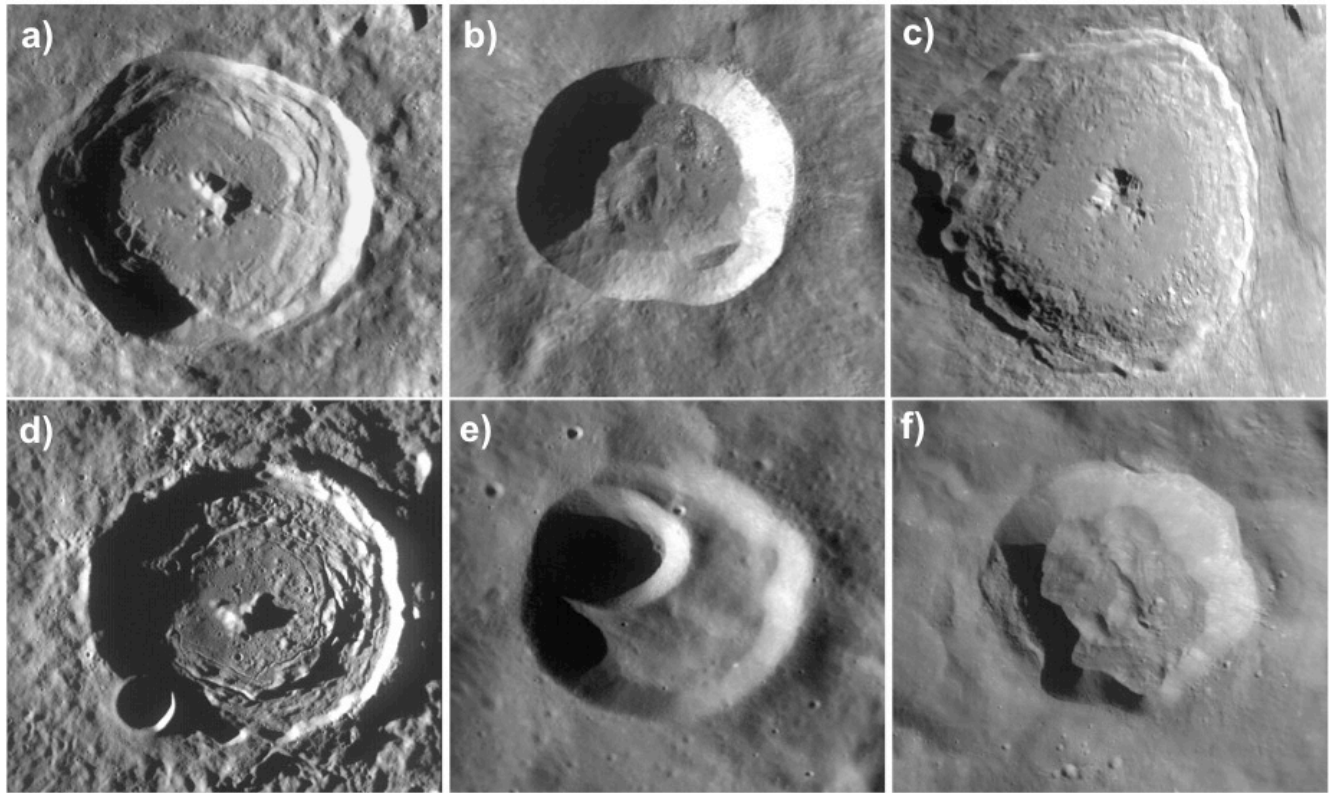


Figure 2 In all images, illumination is from the left, and north is at the top of the image. **a)** Maunder crater (D=55 km) exemplifying a fresh crater with a defined rim, melt pools, and ejecta blanket; **b)** Giordano Bruno crater (D=22 km) exemplifying a fresh crater with a distinct ejecta blanket; **c)** Tycho crater (D= 88 km) exemplifying a fresh crater with clear fault scarps along the western rim and melt pools on the floor; **d)** Taruntius crater (D=56 km) shows floor fracturing interpreted as uplift due to subsurface magmatic activity and thus a crater that is not fresh; **e)** Holetschek Z crater (D=30 km) is not fresh due to an overlying subsequent impact crater **f)** Faraday C crater (D=30 km) is not fresh due to its irregular shape.

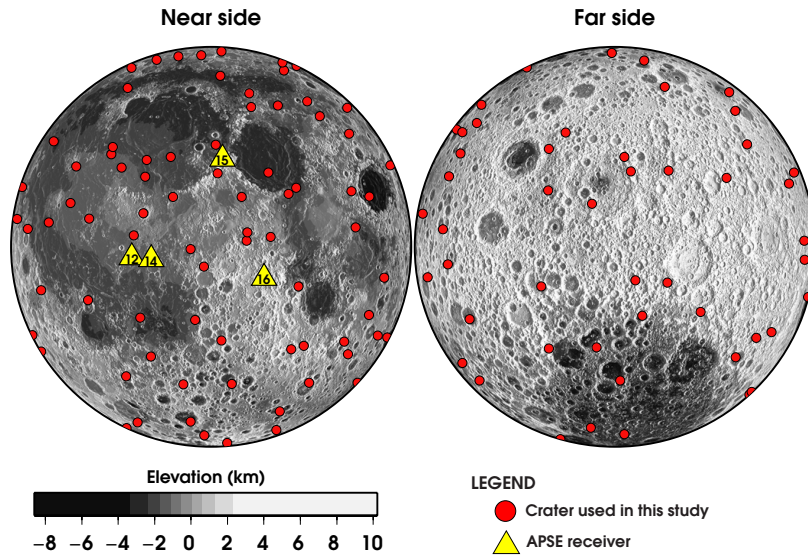


Figure 3 Geographical distribution of the 118 fresh craters studied here. Background is shaded relief map of surface topography using the 4 pixel-per-degree LOLA gridded data. Four of the Apollo landing sites (APSE 12,14,15, 16) are shown for reference.

We also used the WAC images to classify each crater as complex or transitional. Both transitional and complex craters exhibit terraced walls due to slumping of the crater rim, but complex craters should also exhibit a clear central uplift protruding through the melt sheet. We classified craters without a clear central uplift as transitional.

Finally, we identified the terrain type impacted by each crater as mare (M), highland (H), mare-highland border (B), or South Pole Aitken Basin (SPA). This allows us to investigate any systematic variations in crater topography and morphology that might be attributable to differences in the impacted terrain.

2.2 Topography Analyses

We characterize crater topography using the 256 pixel-per-degree LOLA gridded topography, obtained from the Planetary Data System (PDS) Geosciences Node. This was the highest resolution grid available on the PDS at the time we did the analyses, a higher resolution grid (1028 pixels per degree grid) has recently been released. We expect that the higher resolution grid will not significantly affect our results because, as part of our analyses, we confirmed (see Section 3.3) that using the

gridded topography, which is smoothed relative to the individual LOLA tracks, does not bias our measurements, in particular our estimates of central peak heights. The diameter of the central peak, D_{cp} , and the crater rim annulus as a fraction of the crater diameter, D , were identified using Lambert equal area projections of the topography centered on each crater. The crater diameters given in the Losiak et al. (2009) database were compared with the rim crest position observed in the LOLA topography. If necessary the diameter was updated to match that inferred from the LOLA data (Supplementary Table 1). In general, the rim crest lies within an annulus bounded by $0.98D$ and $1.05D$ and, when present, the central uplift lies within a circular region of diameter $D_{cp} = 0.2D$ (Figure 4).

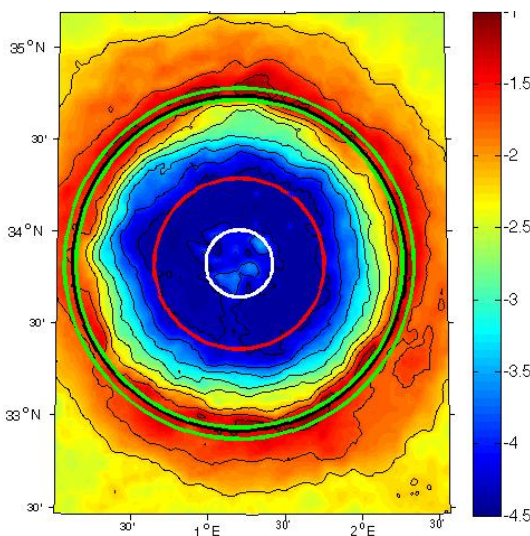


Figure 4 Topography (km) of Aristillus crater showing the central peak region (white circle), the floor region (red circle), and the rim (between green rings). Rings correspond to 0.2, 0.53, 0.95 and 1.1 times the crater diameter (black ring).

For each crater we obtained the rim and floor elevations using a statistical approach. We first identified regions of impact melt in the WAC image, and used the topography of these regions to characterize the floor elevation. This is in contrast to previous approaches that used either an average over the entire crater floor, or single point measurements of the minimum floor depth. The former can introduce a bias to higher floor elevations because of post-impact modification such as slumping, and the latter does not allow an uncertainty in floor elevation to be assigned. Eight of the smaller craters lacked visible regions of impact melt. For these craters we used the topography in an annulus defined

by the diameter D_{floor} , where $D_{\text{cp}} < D_{\text{floor}} < \sim 0.5D$, to estimate the floor elevation. To characterize the rim elevation we use topography measurements within an annulus bounded by $0.98D$ and $1.05D$.

For the floor and rim regions, we produce histograms of elevations, binned in 50m intervals (Figure 4), and examine the distributions and summary statistics such as the mean, mode, median, minimum and maximum. We take the elevation characteristic of the floor (h_{floor}) to be the average of the modal (h_{mode}) and minimum (h_{min}) elevations and assign an uncertainty (σ_{floor}) of $(h_{\text{mode}} - h_{\text{min}})/2$. The rim elevation is characterized similarly, taking the average of the modal and maximum elevation. The crater depth is taken as the difference in floor and rim elevations, with an error equal to the square root of the sum of the squared errors for the rim and the floor.

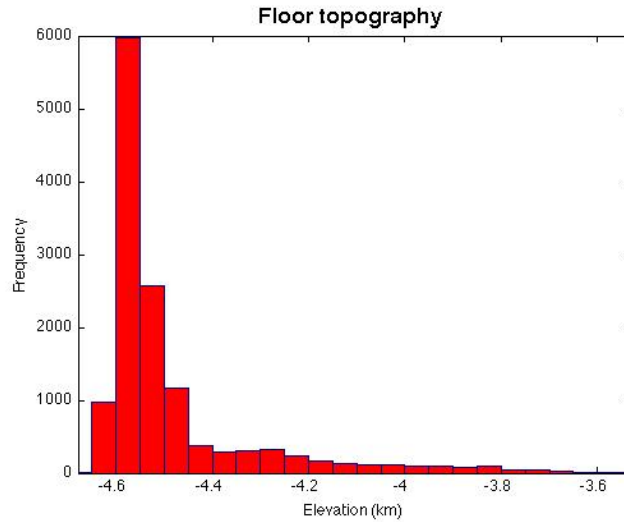


Figure 5 Elevation histogram for floor region of Aristillus crater binned in 50m intervals. The high elevation tail is attributed to the small number of elevations above -2.5 within the central peak region.

Of the 118 craters, 87 display central uplift regions characteristic of complex craters. The central peak height of each of these 87 craters, was calculated by taking the difference between the maximum central uplift elevation and h_{floor} . These central uplift heights are shown as a function of crater diameter in Figure 3. We also determined the surface area and volume of these central uplift regions. Using the gridded topography data, we identify grid cells within a circular region of diameter $0.35 D$ that have elevations greater than a critical base elevation, $h_{\text{base}} = h_{\text{floor}} + f^* \sigma_{\text{floor}}$, where f is a

factor between 2 and 20. f was chosen for each crater individually, to ensure that the central peak region identified in the LOLA topography corresponds to that seen in the WAC image (Figure 6).

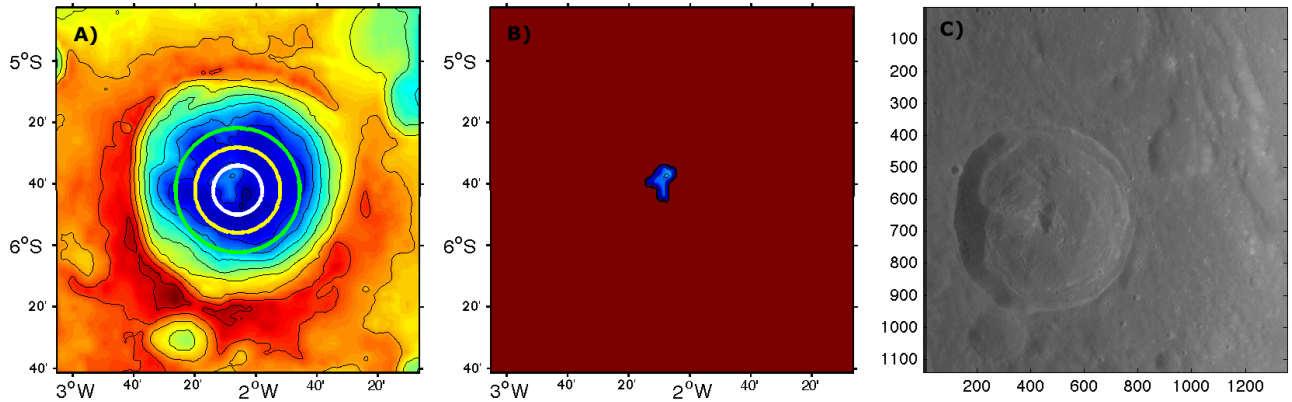


Figure 6 A) 256 ppd topographic map of Herschel crater (5.7°S 2.1°W) using LOLA data. The green, yellow, and white rings indicate a distance from the center of 0.51R, 0.35R, and 0.2R respectively. B) The topography that lies within a 0.35R radius from the center that has a height that is greater than $h_{\text{floor}} + 3 \sigma_{\text{floor}}$ was classified as the central peak topography C) The corresponding WAC image of Herschel used for visual confirmation of the central peak.

As $f > 2$ for all craters, central peak uplifts have elevations that are above the mean floor elevation at the 95% confidence level. Each grid cell contributes a surface area, dA , to the total surface area of the central uplift, and a volume $dV = dA * h$, where h is the elevation of the grid cell relative to h_{base} .

We used LOLA Reduced Data Records (RDR) to obtain tracks across our craters using the JPDA software (O. Barnouin, personal communication, 2011). Topographic profiles were extracted from the GDR along the specific orbit tracks to investigate any differences between the RDR and GDR data. In particular we checked for differences across the crater floor and the central uplift to verify that central uplift heights are not underestimated in the GDR data. Differences between the RDR and GDR profiles along a given orbit track were less than 100 m.

3. RESULTS

We summarize the variations in crater depth and in central uplift height as a function of crater diameter in Figures 8 and 13 below. We distinguish among craters impacting mare, highlands, mare/highlands border and South Pole Aitken terrains, and identify those craters that are Upper Imbrium in age.

Previous studies have reported that the transition from simple to complex craters occurs over the diameter range 15 to 35 km (Pike, 1981) or 10 - 20 km (Head, 1976; Melosh, 1989). We did not attempt to capture the full suite of transitional craters, however Figure 3 shows that in our data set, all craters with diameters in the 15 – 20 km range do not display central uplift regions. Further we see that in the 25 - 45 km diameter range there are both complex and transitional craters, and, with one exception craters with diameters greater than 45 km are all complex.

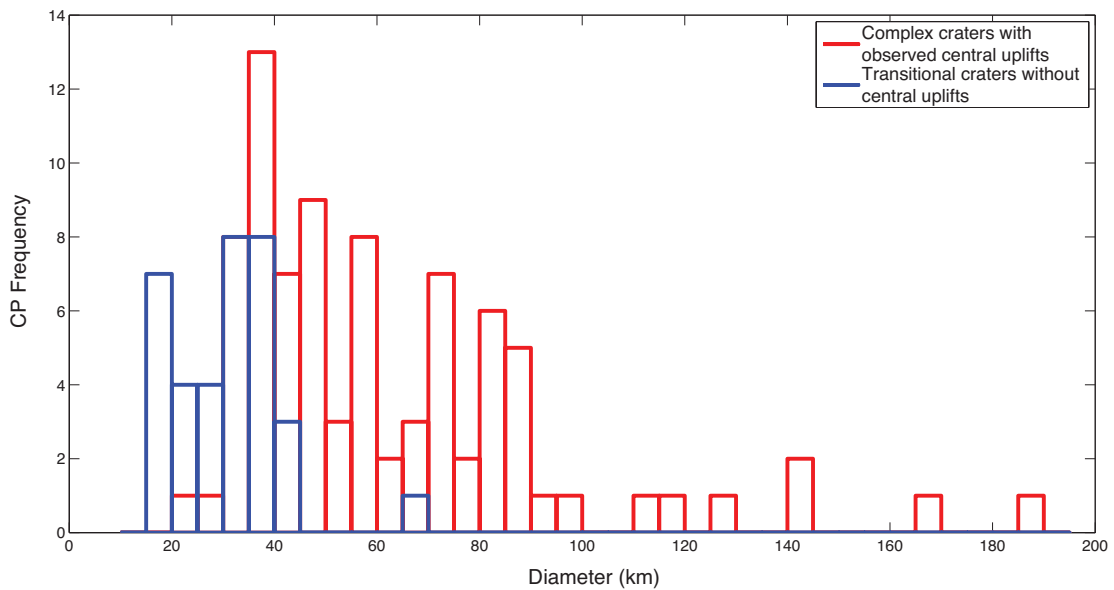


Figure 7 Histograms of craters with or without central peaks in our data set, shown in red and blue respectively.

3.1 Depth - Diameter

Our crater depth-diameter (d - D) results show two trends consistent with previous work. First, as expected, crater depth increases with increasing diameter (Baldwin, 1963; 1965; Pike, 1974; 1977; 1981; Wood and Andersson, 1978). The increase is approximately linear in the log-log domain (Figure 2) suggesting a power relationship between depth and diameter. Second, complex craters on highland terrain are deeper than those on the mare terrain (Wood and Andersson, 1978; Pike, 1980, 1981). The statistical approach used here allows us to estimate uncertainties in crater depths. The depth uncertainty is dominated by variations in the crater rim height. The average variabilities in the floor and rim elevations are 40m and 450m respectively. The largest uncertainties in rim height (and hence in crater depth) are associated with craters that have impacted terrain with significant variations in pre-existing topography.

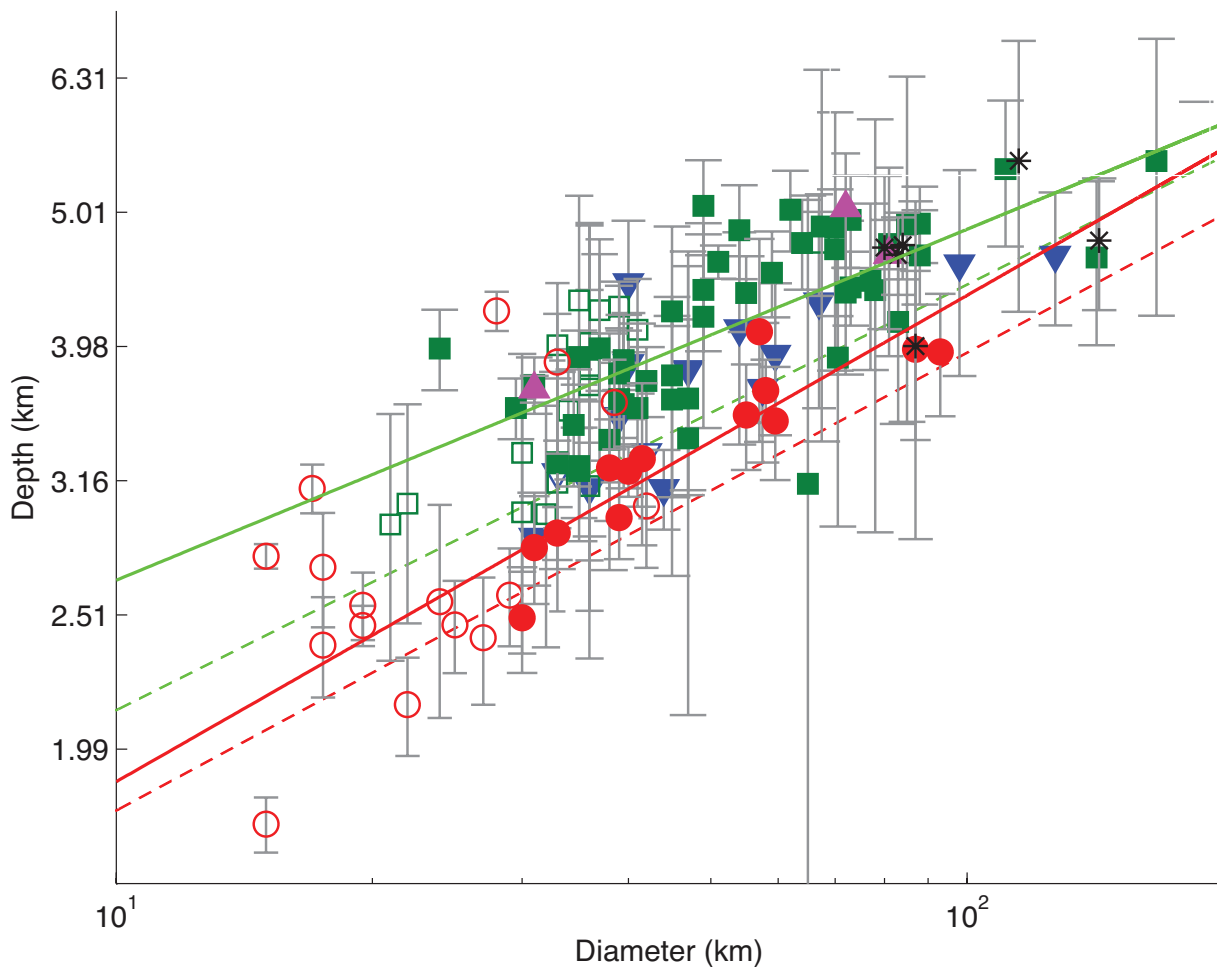


Figure 8 Depth vs. diameter for craters in highlands (green squares), mare (red circles), mare-highland border (blue inverted triangles) and South Pole Aitken (purple triangle). Complex

craters (those with central uplift regions) are shown with solid symbols, transitional craters (terraced walls but no central uplift region) are shown in open symbols. Upper Imbrium age craters are indicated by black stars. Errors in the crater diameter are negligible compared with errors in the crater depth and are not considered here. Solid lines show our depth-diameter relationships for highland (green) and mare (red) craters, and dashed lines show the corresponding relationships of Pike (1981), shown also in Figure 1.

We performed a linear least squares regression in the log-log domain, to obtain power law relationships of the form $d = AD^B$. We determined the constants A and B , the one standard error uncertainties in the model, and the root mean square misfit of the model to the data. Relationships were determined separately for complex craters on the mare and highlands and are reported in Table 1. Our transitional craters, and the Upper Imbrium age craters were not included in the model fits, so our best-fit models are strictly for young, fresh complex craters. The derived power law relationships show that highland craters indeed significantly deeper than mare craters (Figure 4, Table 1). Although we did not include the South Pole Aitken or mare-highland border complex craters in our fits, both of these populations are consistent overall with the fits for the highlands craters.

Table 1 A and B are the constants of the curves fit to the depths and diameters of three subsets of complex craters of the form $d=AD^B$. The root mean square (RMS) misfit of the fit to the observations is also given. Quantities in parentheses are one standard error (s) in each coefficient.

$d=AD^B$	$A (s_A)$	$B (s_B)$	RMS (km)
Highlands $D \leq 180$ km	1.46 (0.02)	0.26 (0.01)	0.42
Mare $D \leq 180$ km	0.82 (0.05)	0.36 (0.01)	0.21

3.2 Central Uplifts

Central peak uplift is seen to increase with increasing crater diameter as observed previously (Wood, 1973; Cintala et al., 1977; Wood and Andersson, 1978; Hale and Head, 1979; Hale and Grieve, 1982), however central peak heights show substantial variability at a given crater diameter. The central peak heights of mare craters appear to be lower on average than those of highland craters over the

same diameter range, although a larger mare crater data set is needed to clearly demonstrate this. For example, the subset of craters with $80 \text{ km} < D < 100 \text{ km}$, has a maximum highland central peak height of 2.6 km (Piccolomini) and a maximum mare central peak height of 1.1 km (Copernicus). Likewise in this subset the maximum highland crater depth is 4.9 km (Hayn and Tycho), and the maximum mare crater depth is 4.0 km (Aristoteles). Given the variability in central peak heights at any given diameter we fit both power law and linear relationships to the central peak heights versus diameter for the mare and highlands regions separately (Table 2). The results indicate that a power law relationship provides a significantly better fit to the observations.

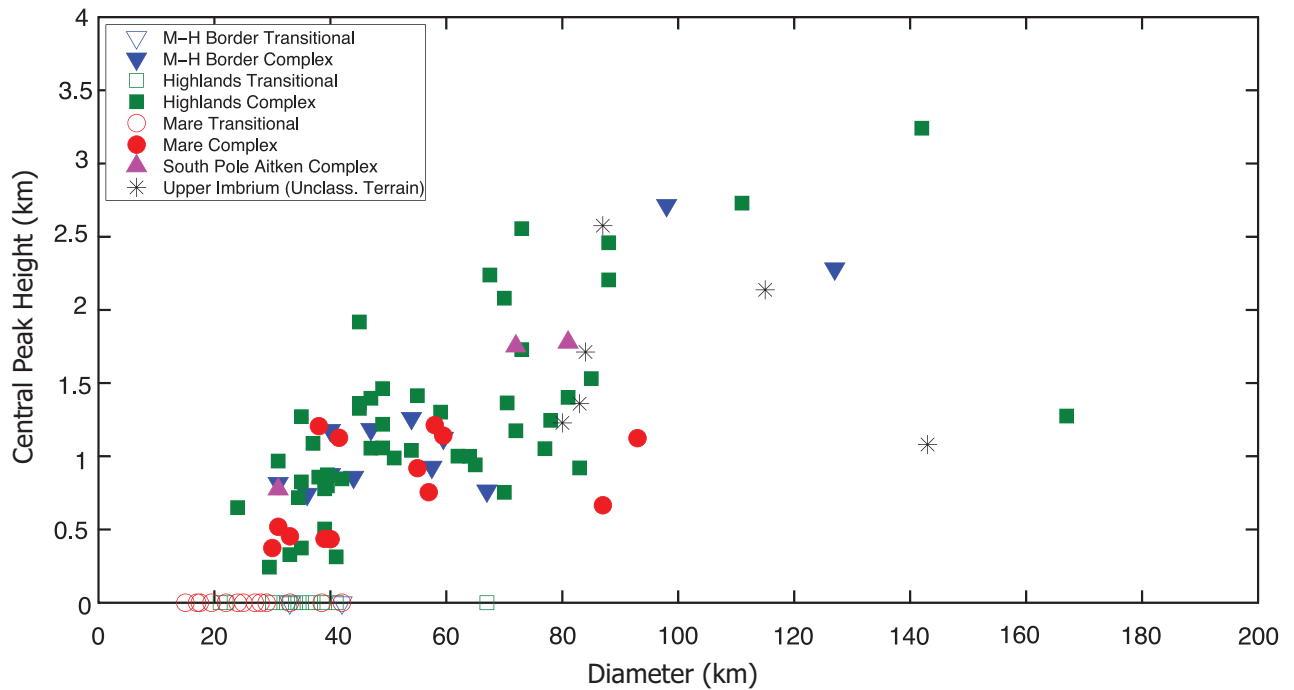


Figure 9 Central peak height vs. diameter for the 87 Copernican or Eratosthenian fresh complex craters with central uplift regions. Symbol color and type as in Figure 7.

Table 2 Results for constants A, B, c and e for power law and linear fits for central peak height versus diameter: $h_{cp} = AD^B$ and $h_{cp} = cD + e$, respectively. The root mean square (RMS) misfits for the fits are also shown.

$h_{cp} = AD^B$	A	B	RMS (km)
Highlands	0.03	0.88	0.50
Mare	0.05	0.69	0.29

$h_{cp}=cD+e$	c	e	RMS (km)
Highlands	0.02	0.38	0.91
Mare	0.01	0.43	0.91

The central peaks show a large range of heights at any given diameter. Examples of 3 craters in the 55 km to 80 km diameter range, with quite different central peak heights each are shown below in Figures 10, 11, and 12. A comparison of the 256ppd LOLA topography (in a) with the WAC images (in b) shows that the different heights are often accompanied by different morphologies.

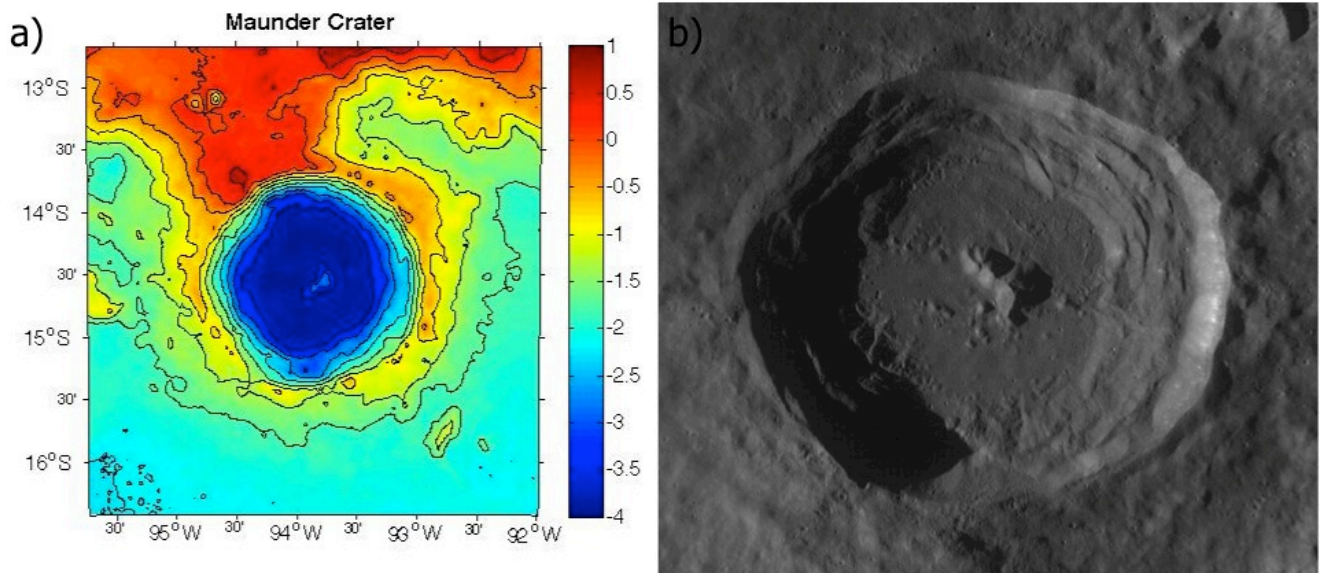


Figure 10 Maunder crater (14.6°S 93.8°W) has diameter of 55km and central uplift height (CUH) of 1.26km. Observations of the crater include a distinct central uplift as well as sharp, continuous terraces along the walls. (WAC #M118104992ME).

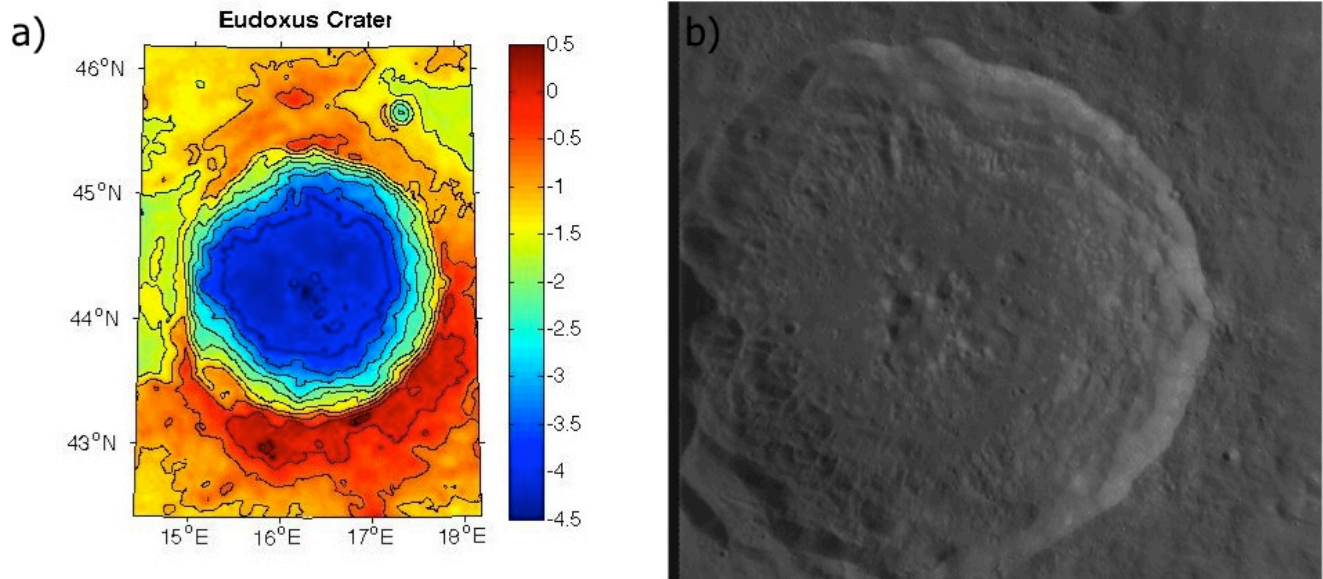


Figure 11 Eudoxus crater (44.3°N 16.3°E) has a diameter of 67km and CUH of 0.76km. Observations of the crater include a central region of several low hills, compared to Maander’s distinct peak, and terraced walls that are less continuous than that seen on Maander. (WAC #M119734736ME)

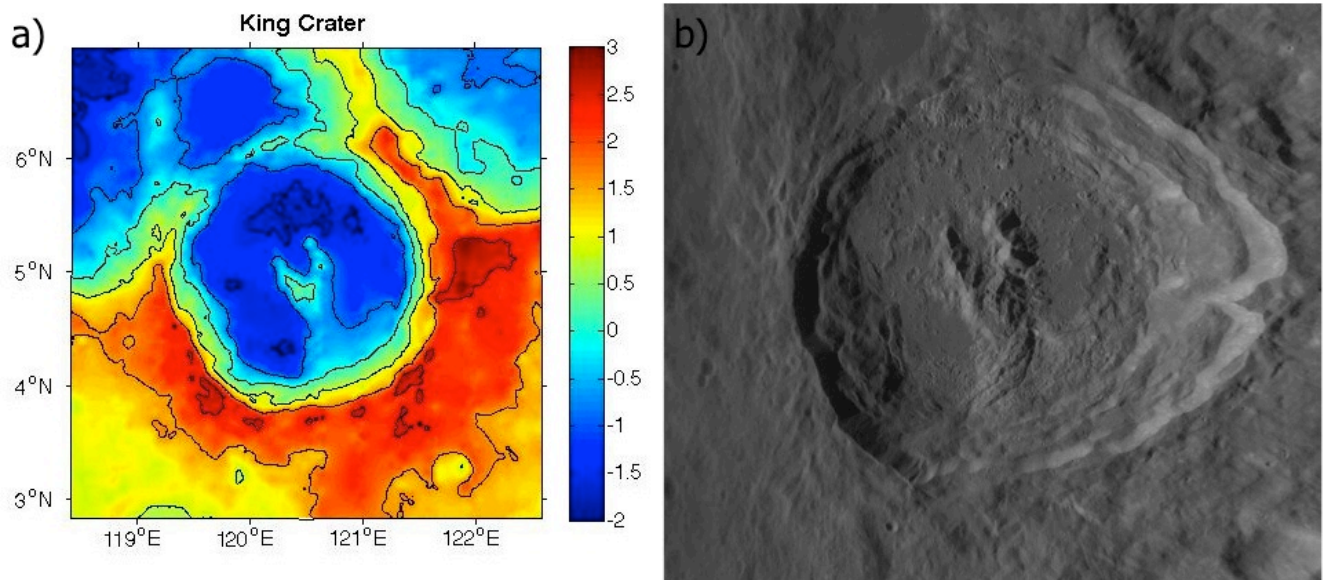


Figure 12 King crater (5.0°N 120.5°E) has a diameter of 76 km and CUH of 2.56 km. Observations of the crater include a U-shaped central uplift region and an asymmetric rim. (WAC #M119062083ME).

3.3 GDR and RDR Differences

In this section we show that using the gridded topography data (GDR) versus individual altimetry orbits (RDR data) does not result in a bias in crater depths or central peak heights. RDR tracks across 20 complex craters were assessed and compared with the gridded data. Differences between profiles extracted from the GDR data and actual RDR profiles were minimal, typically less than 400 m (e.g., Figure 13). Only one crater had a profile where the RDR and GDR profiles differed significantly: one of Copernicus's six central peak profiles varied by 1km.

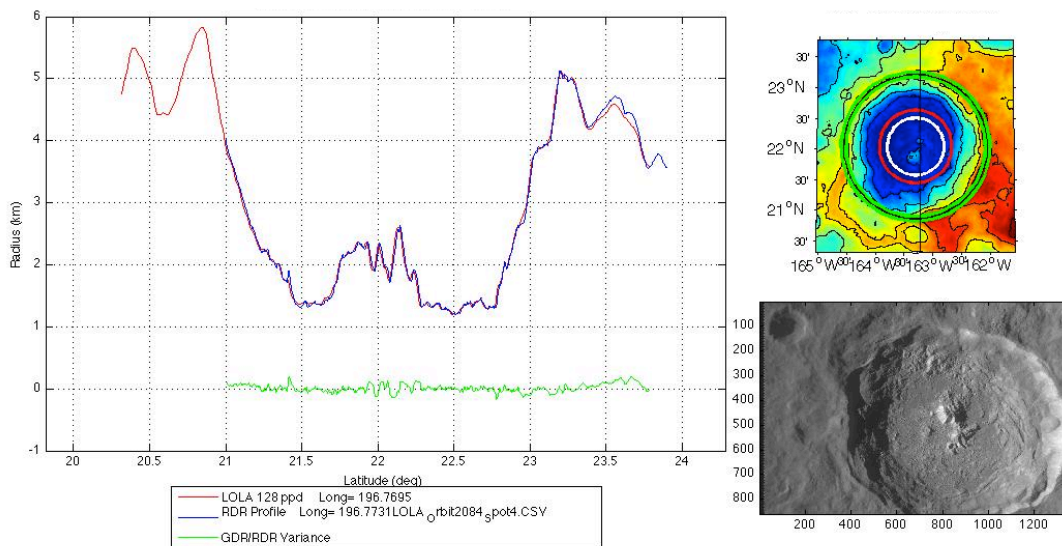


Figure 13 A comparison of the RDR profile across Jackson crater (blue line) to a profile extracted from the GDR (red line). The GDR/RDR difference is plotted below the profile in green. The location of this profile along the crater is displayed on the LOLA projection with a solid black line.

4. DISCUSSION

4.1 Depth – Diameter

Our d - D relationships for the 13 mare and 48 highland complex craters are shown in Figure 8, together with the previously derived relationships of Pike (1981). Complex highlands craters are

significantly deeper than the mare craters as shown by the standard errors on the d - D curves. Highland craters in the 45 km to 65 km diameter range are typically deeper than the best-fit highlands model, but statistical tests showed no evidence for a change in the power law relationship in this diameter range (e.g., from a steeper slope at smaller diameters to a more shallow slope at larger diameters). We find d - D relationships that indicate significantly deeper craters on both the highlands and mare terrain than previously documented in Pike (1981). We examined the data set of Pike (1981): only 12 out of 20 mare craters and 4 out of 37 highland craters in his original data set are now known to be young, fresh craters, and 7 of these are transitional not complex craters (Table 3). The remaining 45 craters of Pike (1981) not used here are likely biased toward a shallower depth due to modifications such as subsequent volcanism, tectonic uplift and infilling due to slumping of the crater walls. We infer that the differences between the current and published studies result from a combination of (1) the inclusion of older and/or modified craters in previous work, and (2) limitations of the stereophotogrammetric and shadow-length data sets used in previous studies.

Five of our large young fresh craters (King, Tycho, Aristoteles, Langrenus and Hausen) were also used in a study of lunar basin depths from Clementine altimetry (Williams and Zuber, 1998). Our depth estimates for four of these craters are up to 10% deeper than those reported in Williams and Zuber (1998), but the differences are less than the uncertainties in the depths. Our data set shows no evidence for a change in the d - D at large crater diameters. However, when combined with 7 larger basins (Figure 4 of Williams and Zuber, 1998), our data are consistent with an inflection in the d - D curve occurring in the 100 km – 200 km diameter range noted in Williams and Zuber (1998).

Table 3 The craters used in Pike (1981) that are now known to be young and fresh.

Name	Highland (H) or Mare (M) “t” denotes a transitional crater
Tycho	H
King	H
Necho	H, t
Conon	H, t
Copernicus	M
Aristoteles	M
Eratosthenes	M
Aristillus	M
Plinius	M
Timocharis	M

Lambert	M
Euler	M
Delisle	M, t
Pytheas	M, t
Dawes	M, t
Bessel	M, t

4.2 Central Peak Anomalies

The LOLA topography data that we use in our study is the first data that is of high enough resolution for one to analyze the central peak heights of complex craters. The results in Figure 9 suggest that target terrain is important, as craters that impact mare terrain seem to have, on average, lower central peaks than those on the highlands. Further, the variability in central peak morphology (WAC images, Fig. 10-12) is interesting and may correlate with the variability in the central peak heights for a given diameter (Fig. 9). A comparison of the central peak heights to depth in Figure 14 shows an increase in variability in central peak heights at crater depths of around 4km. For example for depths between 4km and 4.5km (approximately a 10% variation), central peak heights vary by over 600% ($0.5 \text{ km} < h_{cp} < 3.2 \text{ km}$).

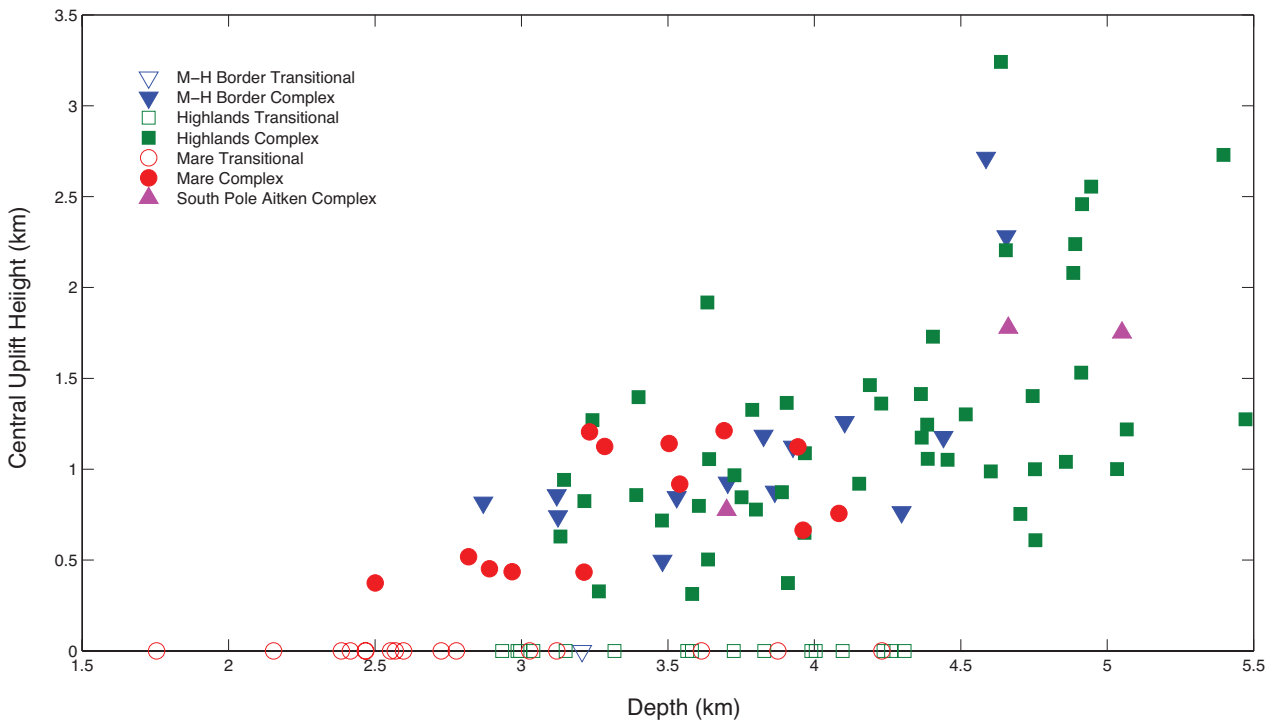


Figure 14 Central peak heights vs. crater depth for the 87 complex lunar craters. Colors and symbols are as in Figure 7 and 9.

5. CONCLUSIONS AND FUTURE DIRECTIONS

With the recently collected LOLA data we can for the first time investigate the absolute topography of lunar complex craters globally. We use a lunar crater database to select young craters from the Eratosthenian and Copernican eras that are greater than 15 km, and identify which of these are fresh using LROC WAC images. Our resulting data set comprises 112 young craters, of which 29, 65, 15, 3 are on mare, highland, mare-highland-border or SPA terrains respectively, as well as 6 older (Upper Imbrium), fresh craters with $D > 100$ km.

We use 256 ppd (~ 30 m spatial resolution) gridded LOLA topography data to estimate the elevation of the crater floors, rims, and maximum elevation of the central peaks. From these we derive the crater rim-to-floor depth and the central peak height (above the crater floor). We find that both d and h_{cp} increase with crater diameter and are well modeled by power law relationships as has been suggested previously. Highland craters are typically deeper and have higher central peaks than those of mare craters. We find no clear evidence for a change in power law relationship for highland or mare crater depths or central peak heights over the diameter range of complex craters. However, there is a suggestion of a change in slope in the depth-diameter relationship for highland craters at around 60 km diameter, and central peak heights show a significant increase in variability at approximately this diameter.

Our results indicate that crater depth at a given diameter is significantly deeper than previously proposed. This primarily reflects differences in the craters used in previously studies compared with those used here. Notably many craters used in previous studies are older and/or modified compared with those used here. Modification would tend to infill or uplift crater floors, as well as reduce the rim elevations leading to shallower depths.

The original terrain impacted has a large effect on the final morphology of the crater. Due to this there is a large variability in rim heights and therefore a substantial variability in crater depths, as shown in Figure 14. Appropriate methods of choosing the rim height need to be further examined in order to minimize this error and to eliminate the bias from the pre-existing topography. In turn this will create a more accurate depth calculation for each crater.

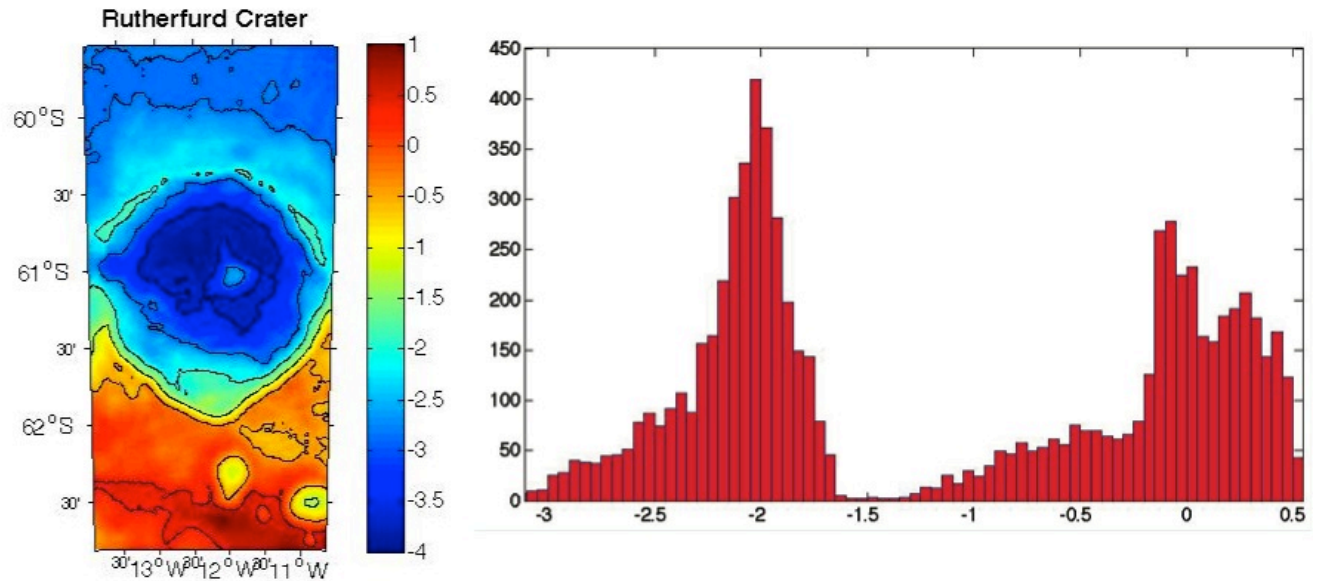


Figure 15 a) LOLA topography of Rutherford crater (60.9°S 12.1°W) b) Rim elevation histogram of Rutherford crater showing two distinct modes corresponding to the north and south topographic dichotomy.

Future studies should look at the large variability within the central peak heights. Correlations of the central peak heights can be made with the differences in central peak shape and morphologies, slopes, mineralogies, and target terrain.

REFERENCES

- Baldwin, R.B. (1963), *The Measure of the Moon*, 488 pp., Univ. of Chicago Press, Chicago.
- Baldwin, R.B. (1965), *The Crater Diameter-Depth Relationship from Ranger VII Photographs*, *Astronomical Journal*, 70(8), 545-547.
- Cintala, M. J., C. A. Wood, and J. W. Head (1977), *The effect of target characteristics on fresh crater morphology: Preliminary results for the moon and Mercury*, *Proc. Lunar Planet. Sci. Conf. 8th*, 3409-3425.

- Hale W.S., and J.W. Head (1979), Central peaks in lunar craters: morphology and morphometry, Proc. Lunar Planet. Sci. Conf. 10th, 2623–33.
- Hale W.S., and R.A.F. Grieve (1982), Volumetric analysis of complex lunar craters: Implications for basin ring formation, J. Geophys. Res., 87, A65-A76.
- Head J. W. (1976), The significance of substrate characteristics in determining morphology and morphometry of lunar craters, Proc. Lunar Planet. Sci. Conf. 7th, 2913-2929.
- Head, J. W., C. I. Fassett, S. J. Kadish, D. E. Smith, M.T. Zuber, G.A. Neumann, and E. Mazarico (2010), Global distribution of large lunar craters: Implications for resurfacing and impactor populations, Science, 329, 1504–1507, doi:10.1126/science.1195050.
- Kadish, S. J., C. I. Fassett, J. W. Head, D. E. Smith, M.T. Zuber, G.A. Neumann, and E. Mazarico (2011), A global catalog of large lunar crater (≥ 20 KM) from the Lunar Orbiter Laser Altimeter, Lunar Plan. Sci. Conf. XLII, abstract 1006.
- Losiak, A., D.E. Wilhelms, C.J. Byrne, K. Thaisen, S.Z. Weider, T. Kohout, K.O'Sullivan, and D.A. Kring (2009), A new lunar impact crater database, Lunar and Plan. Science XXXX, Abstract 1532.
- Melosh, H. J. (1989), Impact Cratering: A Geologic Process, 245 pp., Oxford Univ. Press, New York.
- Mosher, J. (2010), LROC WAC Previewer Software.
http://ltvt.wikispaces.com/Utility+Programs#WAC_Viewer
- Pike, R. J. (1974), Depth/diameter relations of fresh lunar craters: Revision from spacecraft data, Geophys. Res. Lett., 1(7), 291–294, doi:10.1029/GL001i007p00291.
- Pike, R. J. (1977), Size-dependence in the shape of fresh impact craters on the moon, Impact and Explosive Cratering, 489-509, New York: Pergamon.

- Pike, R. J. (1980), Control of crater morphology by gravity and target type: Mars, Earth, Moon, Proc. Lunar Planet. Sci. 11th, 2159–2189.
- Pike, R. J. (1981), Target-Dependence of Crater Depth on the Moon, 12th Lunar and Planetary Institute Science Conference Abstracts, 845–847.
- Wilhelms, D. E. (1987), The Geologic History of the Moon, U.S. Geol. Survey Prof. Paper, 1348.
- Williams, K. K., Zuber, M. T. (1998), Measurement and analysis of lunar basin depths from Clementine altimetry, *Icarus*, 131, 107–122.
- Wood, C. A. (1973), Moon: Central peak heights and crater origins, *Icarus*, 20, 503-506.
- Wood, C. A. and J. W. Head (1976), Comparisons of impact basins on Mercury, Mars and the Moon, Proc. Lunar Sci. Conf., 7, 3629-3651.
- Wood, C. A., and L. Andersson (1978), New morphometric data for fresh lunar craters, Proc. Lunar Planet. Sci. Conf., 9, 3669–3689.